Feasibility study of a positron lifetime spectrometer for measurements of porous and polymer films with a DC positron beam

A. Badertscher, P. Crivelli, A. Rubbia, A.S. Belov, N.V. Golubev, S.N. Gninenko, M.M. Kirsanov, T. Anthonioz, P. Nédélec, D. Sillou, et al.

LAPP-EXP-2004.07
INR-HEP-2004.30

October 29, 2004

Feasibility study of a positron lifetime spectrometer for measurements of porous and polymer films with a DC positron beam.

A.Badertscher[a] , P. Crivelli[a] , A. Rubbia[a] .
A.S.Belov[b] , N.V.Golubev[b], S.N.Gninenko[bd], M.M. Kirsanov[b].
T. Anthonioz[c], P. Nédélec[c], D. Sillou[c], J. Viret[c].
N. Alberola[d], C. Bas[d].

[a] *Institut für Teilchenphysik, ETHZ, CH-8093 Zürich, Switzerland.*
[b] *Institute for Nuclear Research of the Russian Academy of Sciences, Moscow, Russia*
[c] *LAPP, Annecy le Vieux, CNRS-IN2P3, France*
[d] *LMOPS, Le Bourget du Lac, CNRS, France*

Abstract

Positron Annihilation Lifetime Spectroscopy (PALS) is an increasingly important analysis technique that can be efficiently used to characterize the free volume sizes in porous silica and polymer thin films.

In this document a design of a non-expensive lifetime spectrometer to measure positron annihilation lifetime spectra in thin films with a continuous (DC) magnetically guided slow positron beam is described. The system uses secondary electrons emitted from the surface of the sample by the primary positrons in order to generate a START timing signal. Simulation results show that the time resolution can be expected to be $\lesssim 300$ ps at FWHM.

1 Introduction

There is a fundamental interest in studies of polymer surfaces, interfaces and, in particular, of sub-micron thin films of porous silica [1]-[4]. These films have been recently developed as low-dielectric interlayer insulators for use in future high-speed microelectronic devices. Voids are fabricated in these films in order to obtain a high degree of porosity and hence to make the dielectric constant lower. Important pore characteristics of the films, such as average size and size distributions are difficult to measure with standard techniques [5].

A less standard technique, Positron Annihilation Lifetime Spectroscopy (PALS), is well known as an increasingly important tool that can be efficiently used to characterize the free-volume structure of thin films, see e.g. [1]. The technique uses either positrons emitted from a radioactive isotope (so-called classic PALS) or positrons delivered by an intense pulsed positron beam with energy variable typically in the range 1 - 50 keV [6, 7]. The beam based PALS technique has recently been reported as promising for testing pore sizes in the range from 0.3 nm to 100 nm for porous films with a thickness less than 0.1μm [8, 9].

The spectra collected from PALS experiments are usually composed of a number of exponentially decaying functions, attributed to the annihilation of positrons from different states in a sample. Positron annihilation and positronium (hydrogen like bound state of electron and positron) formation and annihilation are responsible for at least three exponentials that characterize the annihilation rate of positrons and *para-* and *ortho-* positronium in a material sample, for illustration see Figure 1.

Orthopositronium (o-Ps), as the most long-lived state, is formed and diffuses to low electron density sites, i.e. cavities or holes, in polymers. The annihilation of orthopositronium implies a pick-off process of an electron in the void or pore walls by the positron involved. The lifetime τ_3 of o-Ps in the sample is directly correlated to the radius of free-volume holes (R_f) through the following equation [1]:

$$\tau_3 = 0.5\big[1 - \frac{R_f}{R_f + 1.66} + \frac{1}{2\pi} sin\big(2\pi \frac{R_f}{R_f + 1.66}\big)\big]^{-1} \qquad (1)$$

Therefore, this relation provides the *key* physical information concerning free volumes in thin films. As one can see from Eq.(1), in order to be sensitive to the pore size of the order of $\simeq$ 10 Å the corresponding exponential with the lifetime of the order of $\tau_3 \simeq 1$ ns has to be resolved in a PALS spectrum.

In classic PALS setups the timing start signal t_0 is provided by a $\gamma-$ray that is released coincidentally from a radioactive source (typically ^{22}Na) with the positron. The stop signal is provided by one of the annihilation γ-rays. The *advantages* of this type of PALS technique are a high counting rate and a relatively simple experimental apparatus. The *disadvantage* is that the positrons are implanted relatively deep and in an uncontrolled fashion, so that only *average* properties of a sample can be studied with such a technique. Thus, this scheme is well suited for the investigation of the

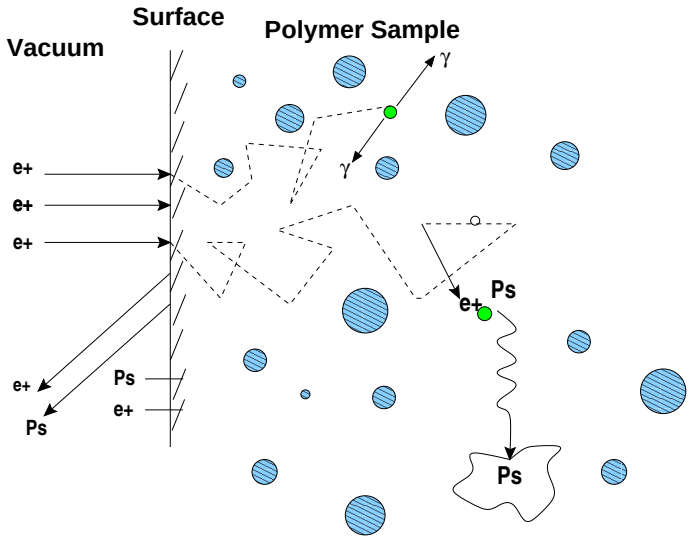

Figure 1: *A schematic diagram of the positron and Ps states in polymer sample.*

bulk materials, but not for the thin-film samples.

In contrast, the *major advantage* of the PALS beam technique is the ability to control positron implantation into the sample. The sample can be depth-profiled by varying the incident beam energy [1]. The timing start signal is provided either by the pulsing system of the positron beam, or by secondary electrons produced when the positron beam strikes the sample surface [6]. In the first case, despite the high performance reached [10, 11], the quite high cost and complexity makes it unaffordable for small laboratories. The latter case is a relatively simple and low cost one. It is based on the use of an appropriate detector (e.g. a microchannel plate) to detect secondary electrons and to generate the start signal t_0. The stop signal is still provided by one of the annihilation γ-rays. Both techniques are relatively new, which hold great promise, particularly in the study of void formation in thin films [1]. These techniques have been used to determine the free-volume hole size distribution in various thin-film materials (e.g. polymers, porous SiO_2, ..) as a function of growing conditions, temperature, pressure, etc... [12].

The rest of this paper is organized in the following way. In Section 2 the detailed description of the proposed PALS detector used for a continuous slow positron beam is given. Preliminary simulation results and performance of the detector are discussed in Section 3 and the trigger rate is evaluated in Section 4. Section 5 contains concluding remarks.

2 Experimental setup

The experimental setup is designed with the goal to observe the exponential components in the positron lifetime spectra, if their intensity is greater than a few % (for a typical statistics of 10^6 events in the spectrum) and the lifetime is greater than a few hundred psec. Figure 2 shows a schematic view of the PALS detector. The positrons from a continuous slow positron beam are stopped in a sample and either form positronium, i.e. $o-Ps$ or $p-Ps$, or annihilate promptly into 2γ's. The secondary electrons (SE) produced by positrons hitting the target are accelerated by the positive voltage applied to the grid relative to the grounded sample and the transport tube. They are transported by a magnetic field in the backward direction relative to the positrons, moving in spirals along the magnetic field lines, and are deflected to a micro-channel plate (MCP) by a $E \times B$ filter as shown in Figure 2. The trigger for the data acquisition and START signal t_0 are generated by the pulse from the micro-channel plate used as a detector of secondary electrons.

Accordingly, the apparatus consists of several distinct and separated parts: i) a slow positron beam with energy range $\simeq$1-50 keV; ii) a high signal-to-noise ratio positron t_0 tagging system, based on secondary positron detection with a high performance MCP, iii) a photon detector, viewing the sample chamber. For efficient detection of annihilation photons, the sample chamber has as little wall mass as possible to minimize photon energy absorption.

To achieve a high sensitivity of the PALS detector, several factors, in particular for designing the part ii) and iii), are of great importance:

- The time resolution of the start-stop spectrum must be in the range 200-400 ps (FWHM),
- The shape of the time spectrum must be as close as possible to a Gaussian. The ratio of $R = Peak/Noise$ should be $R > 10^3$ or better,
- The rate of trigger events per second, i.e. coincidences of MCP and γ-signals, should be as high as possible, thus, requiring good secondary electron and photon detection efficiencies and a relatively small dead time. For a typical slow positron beam intensity of $\simeq 10^5$ e^+/s the trigger rate is expected to be $\simeq$ 1-10 kHz which is low enough to allow these events to be recorded without losses.

The system works in detail as follows: the continuous beam of positrons with energy $\simeq$ 1-50 keV is guided by a magnetic field created by coils with a typical value of $B \simeq 100$ G and passes through a region with crossed electric and magnetic fields, i.e. the $E \times B$ region in the schematic diagram of Figure 2. The transverse electric field has a value $E \simeq 20$ V/mm, the length of the filter is $\simeq 50$ mm. Positrons drift in the crossed electric and magnetic fields with a velocity given by

$$\mathbf{V_d} = \mathbf{E} \times \mathbf{B}/B^2 \tag{2}$$

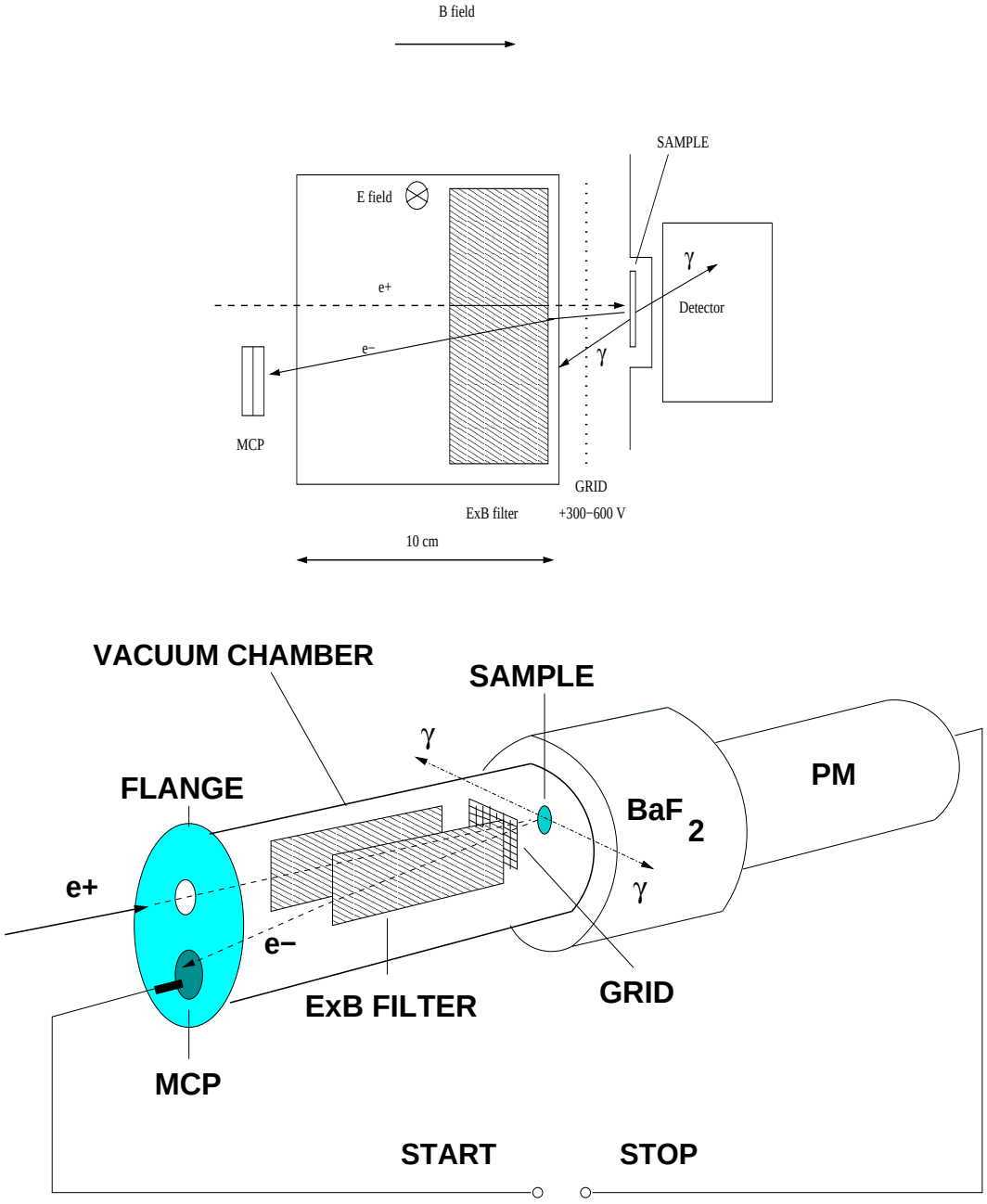

Figure 2: *Schematic illustration of the lifetime spectrometer for the PALS measurements.*

For given values of the electric and magnetic fields the drift velocity is $V_d = 2 \times 10^3$ m/s resulting in a positron displacement of about a few cm in the drift region 1. Then, positrons are transported to the sample by the magnetic field. The sample is a disk with a diameter of $\simeq 10$ mm and a thickness of 0.1 μm. The SE acceleration potential of -300 V is applied to the grid. The MCP front face, as well as the adjacent aperture, are also set to +300 V. This prevents the electrons from slowing down, which would increase the spread of their time-of -flight. The secondary electrons are transported in the backward direction relative to the positrons, see Figure 4, moving in spirals along the magnetic field lines. Thus, trajectories of the secondary electrons will be spatially separated from the positron trajectories by a distance estimated to be $\simeq 25$ mm, significantly larger than the diameter of the positron and test electron beams of about 5 mm. The background count rate of the MCP can limit the efficiency of the positron tagging. This and other sources of background can be suppressed by an appropriate choice of the MCP type and/or by using a positron beam in a pulsed mode with a low duty cycle. Preliminary results illustrating the method are shown in Figure 4, where the calculated trajectories of positrons and secondary electrons passing trough the $E \times B$ filter are presented. The details of Monte Carlo simulations are described in Section 3.

The MCP Hamamatsu F4655-12 is selected for the tagging system, because it provides the best signal-to-noise ratio. This type of MCP detector has two plates with an active area of 18 mm and a fast time response. The MCP signal rise time is $\simeq 300$ ps, while the transit time spread is less than 100 ps. The signal amplitude varies typically from 0.1 to 1 V depending on the applied voltage, the MCP gain (typically greater than 10^7) and the number of the emitted SEs. The collection voltage between the MCP bottom surface and the anode is not critical, a setting above 100 V is sufficient for $> 95\%$ collection efficiency. The MCP detector is assumed to be connected through a $\simeq 100$ pF capacitor. Special care is needed to obtain as clean as possible reflection-free output pulses.

The sample surface could be coated by 10-20 nm of Cu for an efficient sample surface discharging and higher secondary electron emission coefficient [16], other coating materials can also be considered. In this case, for positron energies greater than $\simeq 2$ keV, the mean implantation depth is greater than 10 nm, and most of the positrons diffuse to the film surface, since the diffusion length is also greater than 10 nm.

To ensure a minimal probability of total absorption of annihilation photons, the target itself and the surrounding components of the target region must be carefully designed. To minimize the thickness of dead material, in particular the thickness of the beam pipe in this region is important. Based on simulation results a few mm thick stainless steel pipe seems to be the best choice.

Because of the presence of the magnetic field and due to the required good timing performance, the choice of the components for the photon detector is quite limited. For studies with polymeric systems, BaF_2 scintillators can be used together with Hamamatsu H2431 PMTs, which incorporates a borosilicate glass window. The

CFDD's could be the Canberra 2129 module and the TDC could be the Canberra 2145. The film samples might be inserted into a Cryostat to allow the temperature control.

Data acquisition for the PALS spectrometer is controlled through a single computer connected to the system. Typically, 10^6 counts are collected per spectrum, which are analyzed using, e.g. the PATFIT-88 software package [28].

In order to achieve the best timing resolution, the contribution from scintillator-PM system has to be minimized. For this reason, the following questions have to be studied in the future:

- Type of scintillators, their size, wrapping material, and type of the contact to the photomultiplier;
- Type of photomultiplier's, high-voltage distribution along the dynode system, fast signal electronic chain; high frequency preamplifier's, after-pulses;
- Type of the fast/slow electronics, CFDD, TDC, energy selection;
- Intensity, counting rate and pile-up effect;
- Need and type of the magnetic shielding,
- Monitoring and calibration; long-term stability of the spectrometer;
- Sample holder correction and method to apply them;
- Program for the deconvolution of the PALS spectra taking into account the shape of the resolution function, see e.g. [31]. Cross-check with the Monte Carlo simulation.

3 Monte Carlo simulation

Typically, the Monte Carlo method is a very powerful and reliable procedure to study the performance of a detector design in particle physics. In this work, Monte Carlo simulations are also used as an important tool to evaluate the performance of the PALS detector and to estimate contributions from different sources of systematic errors and statistical uncertainties which might affect the accuracy of the PALS lifetime spectra decomposition.

The program is based on the BField-3d package used to calculate field maps [15] and the GEANT 3.21 package to calculate particle transport in these fields and particle interactions with the sample and detectors [20]. The flow chart of the Monte Carlo simulations is schematically shown in Figure 3. The following features and physical characteristics of the PALS detector are introduced into the Monte Carlo program:

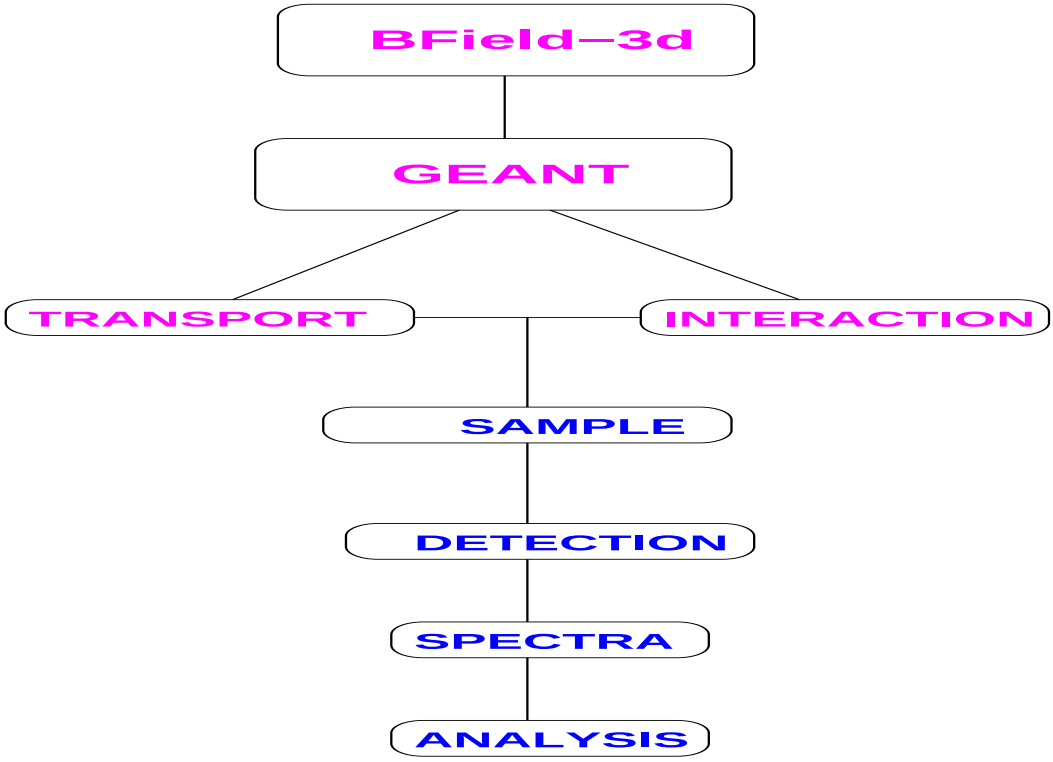

Figure 3: *Flow chart of the Monte Carlo simulation.*

- The geometry of the experimental set-up and the composition of materials, close to the one shown in Figure 2
- E, B field map calculations
- Particle transport in these fields
- The positron slowing-down processes while colliding with the sample material, taking into account the dependence on the positron incident angle at the sample
- A simple approach to simulate secondary emission from the sample surface
- γ-interactions in the scintillator detector and various non-active materials surrounding the source and the region of the sample

The disadvantage of the Monte Carlo method is a large CPU time required by computations. This is because the precision of the numerical calculations strongly depends on the number of steps and simulated trajectories, the energy threshold of secondary particles traced in the simulation, etc... For this reason and for the sake of simplicity some distributions, e.g. such as for secondary electrons, were parametrized based on available data. The number of simulated events was compromised between the CPU time and the required precision of computations.

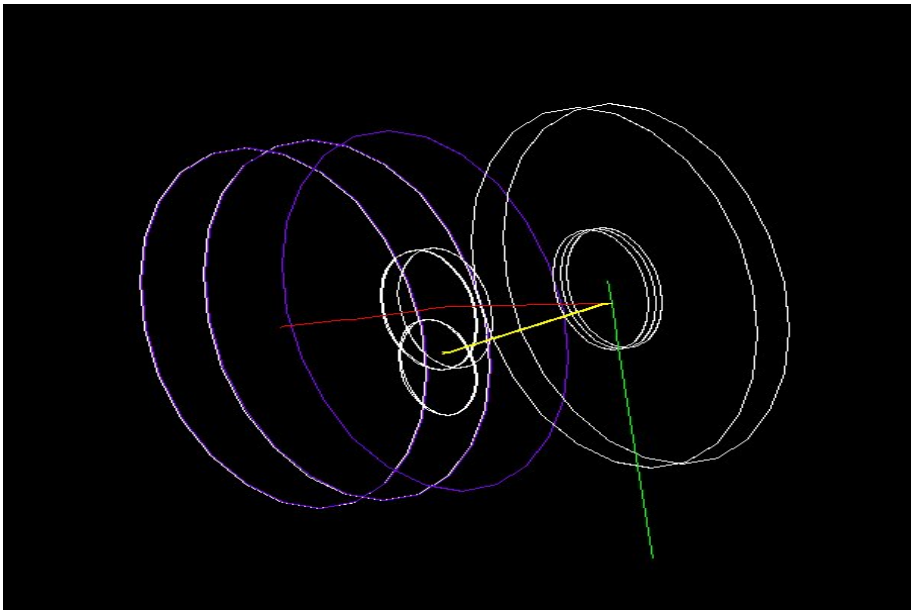

Figure 4: *Calculated trajectories of incident positrons and secondary electrons in the PALS detector. The vertical line represents annihilation photons.*

3.1 Positron transport

The magnetic field map was carefully simulated by the BField-3d package and cross-checked with available measurements of coil prototypes. Then, the magnetic field map was implemented into GEANT 3.21 and positron trajectories were simulated with this package [20]. An example of calculated trajectories of an incident positron and secondary electron in the PALS detector for a single simulated event is shown in Figure 4.

The 1D-, and 2D- spacial distributions of positrons in the X-Y plane transverse to the beam axis at the entrance to the $E \times B$ filter and at the sample position are shown in Figures 5 and 6, respectively. One can see that in accordance with Eq.(2) the drift of positrons in the vertical direction along the Y-axis is of the order 20 mm for an initial positron energy of 2 keV.

3.2 Secondary electrons (SE)

To avoid problems due to the very large amount of computer time required for a secondary electron simulation, the energy spectrum of secondary electrons was taken from refs.[16], the angular distribution was assumed to be isotropic, as schematically illustrated in Figure 7.

The SE emission is a surface effect, involving only a very thin layer of the sample material in the process. Thus, the SE yield and hence the MCP output signal are pro-

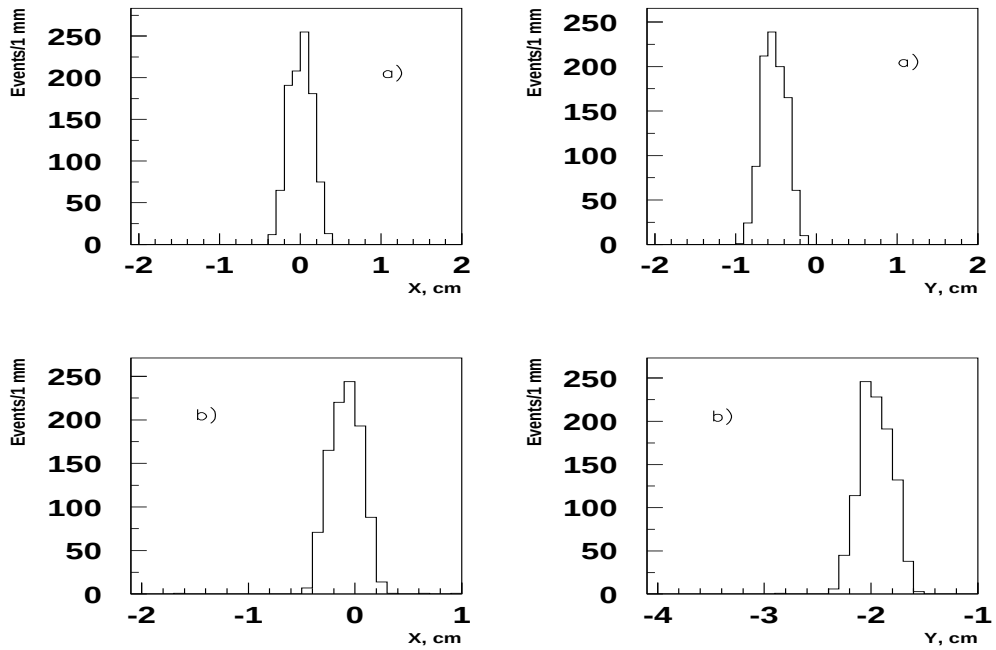

Figure 5: *X- and Y-distribution of positrons a) at the entrance of the $E \times B$ filter and b) at the sample.*

portional to the energy loss *dE/dx* of the positron. This yield and the corresponding energy spectra of SEs are quite important for the performance of the tagging system and its efficiency.

The simulated distribution of kinetic energies of secondary electrons emitted from the Al sample hit by positrons with kinetic energy of 2 keV is shown in Figure 8.

The positron induced secondary electron emission spectra are consistent with data [16] and, in addition, are planned to be cross-checked with future measurements at an electron and positron beam. The distributions are dominated by a broad peak from zero to a few eV energy. The tail in the distributions of the longitudinal energy up to $\simeq$ 10 eV is reported in the literature, see e.g. [17], and is included in the simulation in order to see its effect on the width and shape of the START-STOP time spectra.

The 1D-, and 2D- X,Y-distributions of secondary electrons at the entrance to the MCP are shown in Figures 9 and 10, respectively.

Note, that secondary electrons are accelerated away from the sample by an electric field applied between the sample and the grid, see Figure 2. The same electric field accelerates positrons passing through the grid, which follow trajectories almost perpendicular to the surface of the sample. The corresponding distribution of the incident angle with respect to the normal to the sample surface is shown in Figure

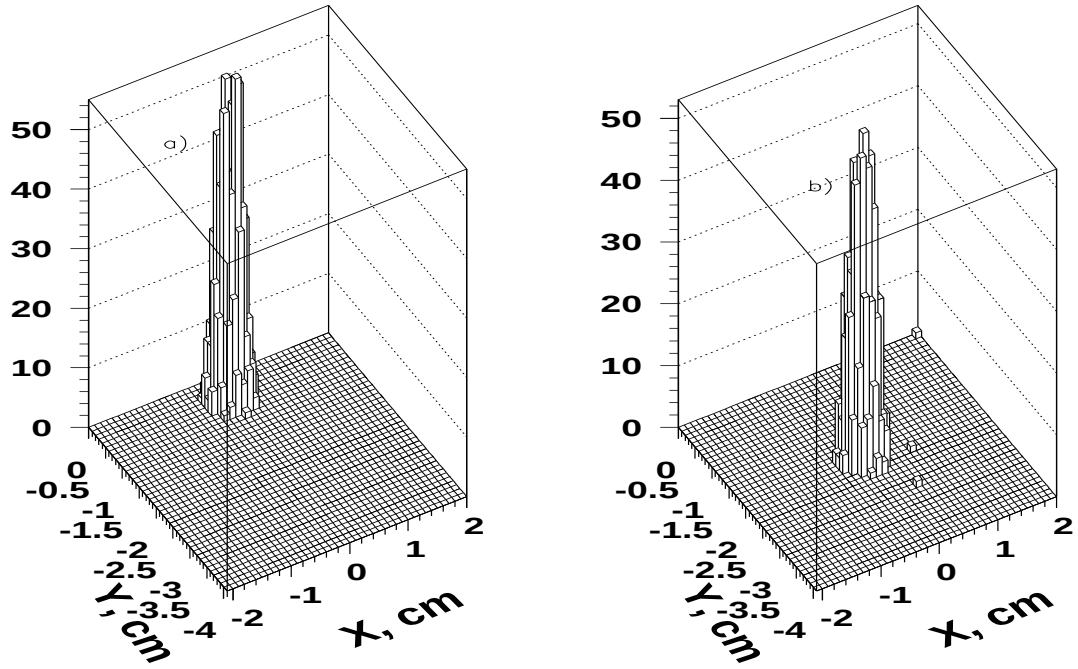

Figure 6: *Two dimensional X-Y distribution of positrons a) at the entrance to the $E \times B$ filter, and b) at the sample.*

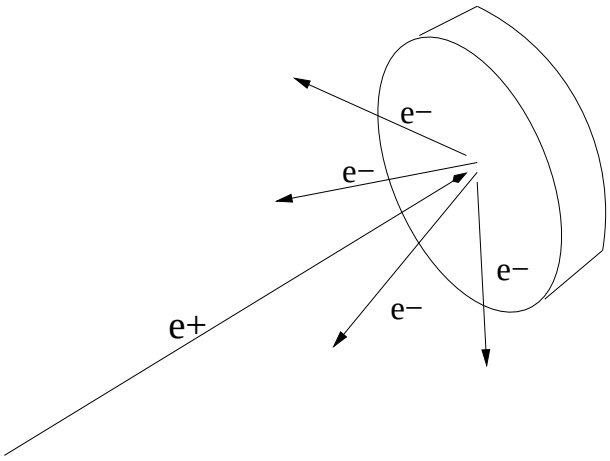

Figure 7: *Schematic illustration of the isotropic distribution of secondary electrons emitted from the sample.*

11. As one can see the average incident angle is different from zero. The deviation of the average implantation depth due to this effect, from the mean depth predicted by

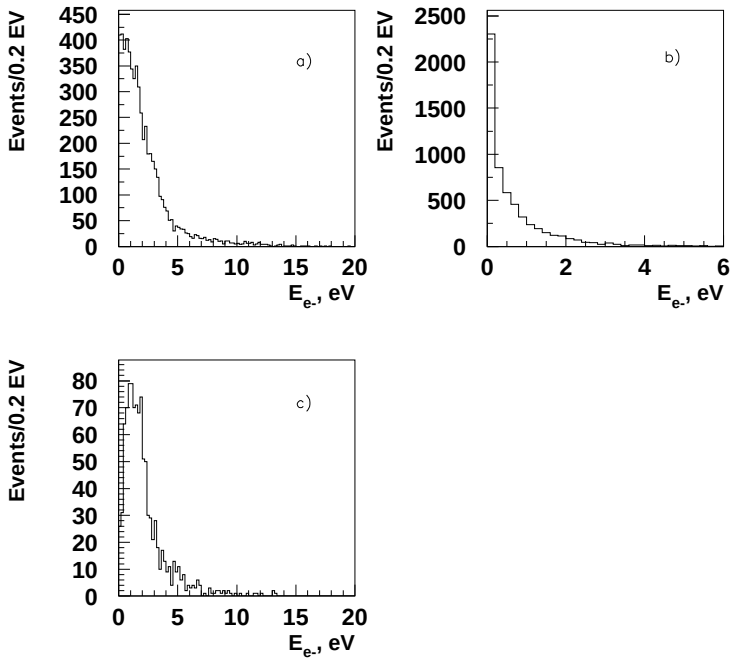

Figure 8: *Distributions of the kinetic energy of secondary electrons emitted from an Al target after the target was hit by a 2 keV positron a) total kinetic energy, b) longitudinal energy, and c) longitudinal energy of the first secondary electron emitted from the target.*

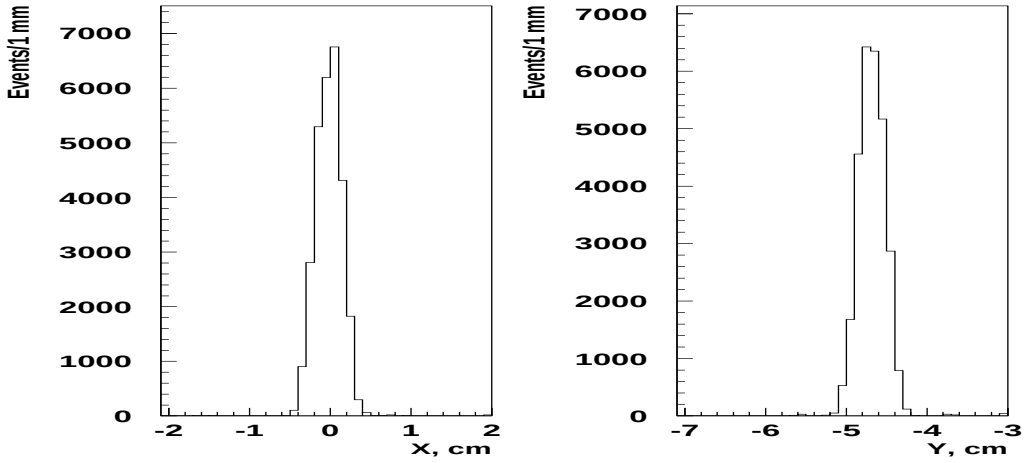

Figure 9: *X- and Y-distributions of secondary electrons at the MCP.*

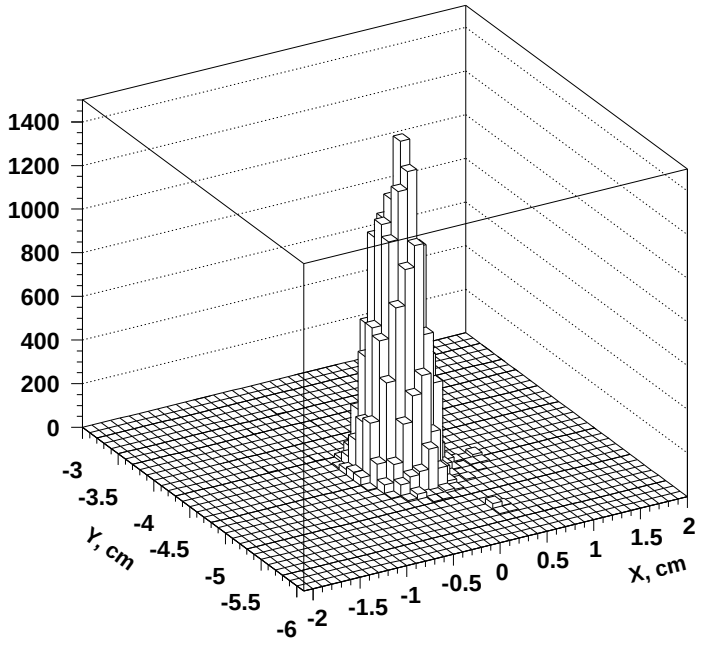

Figure 10: *Two dimensional X-Y distribution of secondary electrons at the MCP.*

the Makhov expression (see e.g. [6]), was found to be negligible for the values of the E- and B-fields used in the detector.

3.3 Shape of the time spectrum and time resolution

The Monte Carlo simulations of the time-of-flight of secondary electrons were also carried out to evaluate the effect of the time resolution of the PALS detector. In this simulation the geometry of the detector was close to the one shown in Figure 2 and the values of the electric potential and magnetic field were the same as indicated in Section 2. The t_0 START signal was defined as the arrival time of the first secondary electron hitting the MCP detector surface.

The time of flight distributions for secondary electrons arriving at the MCP calculated for two accelerating gaps $L = 20$ and 1 mm between the grid and the Al sample, are shown in Figure 12. The distributions are slightly asymmetric and have left tails. The origin of these tails is related to the high energy tail in the distribution of the longitudinal kinetic energies of secondary electrons emitted from the sample, which is shown in Figure 8. These electrons arrive faster at the MCP. The correlation between the initial longitudinal kinetic energy and the arrival time at the MCP is shown in Figure 13. As one can see, the larger L, or SE's time-of-flight, the larger

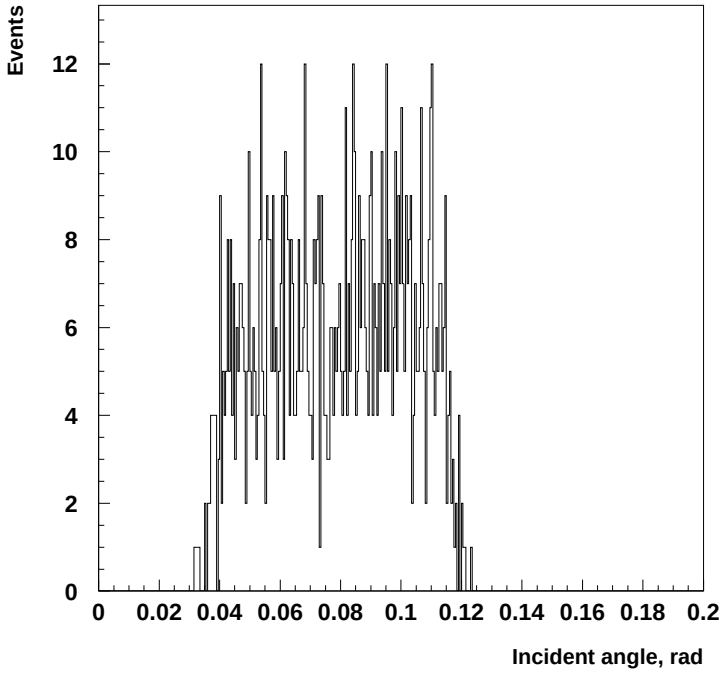

Figure 11: *Distribution of incident angles of positrons at the target.*

the dispersion of electron arrival times at the MCP. To reduce this effect, the SEs should be accelerated by the electric field between the grid and the sample as much as possible and during as short a time as possible after the production.

The most important result of these simulations is that the time spectrum has an asymmetry, which indicates the sensitivity of the spectrum shape on the initial energy and emission angle distributions of the secondary electrons. Obviously, these spectra depend also on the atomic number Z of the sample material and on its surface condition under vacuum.

One of the main factors which contributes to the timing resolution is the γ- detector (i.e. scintillator-photomultiplier (PMT)) resolution. The best timing resolution of a single good PMT coupled to the BaF_2 crystal (about 500 cm^3 in volume) is of the order of 200 ps at FWHM. Convoluting this value with the best SE time-of-flight spread obtained for $L = 1$ mm, one can evaluate the overall timing resolution of the PALS detector to be about ≈210 ps (FWHM).

Additional factors that can affect the timing resolution and the sensitivity of the PALS detector are

- The coefficient of secondary electron emission;
- The efficiency of the electron transport from the target to the MCP, and the

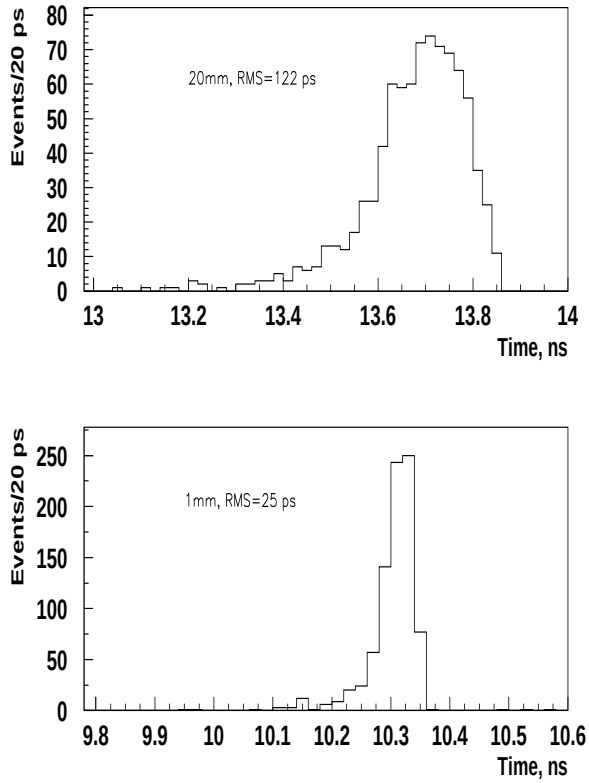

Figure 12: *Examples of time-of-flight distributions of secondary electrons emitted from the Al sample at the MCP detector, calculated for accelerating gaps of 20 and 1 mm, respectively.*

efficiency of the MCP itself;

- The MCP noise level, and the environmental and physical backgrounds, e.g. from beam interactions with residual gas and cavity walls, with material of the $E \times B$ filters etc. accompanied by electron or ion production.

A precise evaluation of their contribution is not easy to simulate, however, one can estimate the final result for the time resolution to be comparable to $\simeq 210$ ps. In this estimate we neglect the jitter of the MCP detector itself, since it is much smaller than $\simeq 100$ ps [30].

One of the advantages of the considered PALS detector scheme is the absence of corrections related to the source holder or capsule. However, the shape of the START - STOP spectra might suffer from distortions due to positrons back scattered from the sample with their subsequent annihilation in the surrounding materials. The

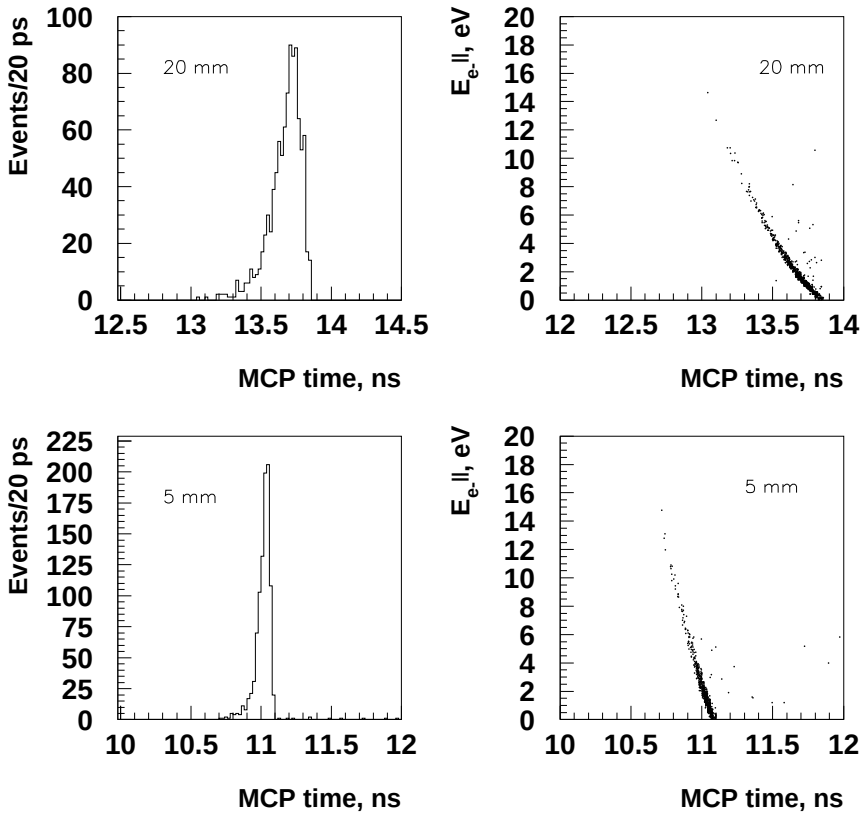

Figure 13: *Time distributions of secondary electrons at the MCP detector and two-dimensional distributions of the arrival time at the MCP vs.longitudinal kinetic energy of secondary electrons on the target for the accelerating gap of 20 and 5 mm, respectively.*

preliminary Monte Carlo simulations show that one of the largest contributions to the parasitic shape of the timing spectrum is expected from the annihilation of positrons back scattered at the acceleration grid. Thus, the transparency (i.e mesh sizes) and position of the grid have to be further optimized. One possible way to solve the problem is to construct specially designed electrodes instead of a grid with as little dead material as possible.

4 Trigger Rate

The trigger rate R in the detector is given by the following formula:

$$R = N_{e^+} \times P(k, \epsilon_t, \epsilon_{MCP}) \times \epsilon_\gamma \tag{3}$$

where $N_{e^+},\ P(k, \epsilon_t, \epsilon_{MCP}),\ k,\ \epsilon_t,\ \epsilon_{MCP},\ \epsilon_\gamma$ are the beam intensity, overall detection efficiency of the MCP START signal, average secondary emission coefficient, SE transportation efficiency, MCP detection efficiency, and the efficiency of the photon-detection by the γ-detector, respectively.

Numerically, for $N_{e^+} \simeq 10^5 Hz,\ k \simeq 2.5\ \epsilon_t \simeq 0.5,\ \epsilon_{MCP} \simeq 0.6,\ \epsilon_\gamma \simeq 20\%$, one gets a trigger rate

$$R \simeq 1 - 10kHZ$$

In the above Eq.(4) it is assumed that the number of electrons arriving at the MCP per time interval has a Poisson distribution, and that the START signal is generated by the first secondary electron.

The accidental event rate collected within a PALS spectrum is given by the formula:

$$n_{acc} \simeq n_{start} \times n_{stop} \times \Delta\tau \tag{4}$$

where n_{start} and n_{stop} are the Start, Stop counting rates, respectively, and $\Delta\tau$ is of the order of the longest lifetime component of the PALS spectrum $\Delta\tau \simeq 1$ ps. For typical values $n_{start} \simeq 10^4/s,\ n_{stop} \simeq 10^4/s$ and $\Delta\tau \simeq 1$ ns, the value $n_{acc} \simeq 10^{-1}/s$ or $\simeq 10^{-5}$R.

5 Summary

We described the design of a relatively simple and compact lifetime spectrometer for the measurements of porous or polymer thin film characteristics with the Positron Annihilation Lifetime Spectroscopy by using a DC magnetically guided positron beam.

Several effects which might influence the precision of the measurements are simulated and discussed. The most important one, requiring further investigation, is that the PALS time spectrum could have a slight asymmetry caused by the initial energy and emission angle distributions of secondary electrons. There are also several other questions concerning this technique that need to be studied. Among them, the most important are:

- How to eliminate or to take into account the back scattering effect?
- How many positrons do not annihilate in the sample and how do they affect the PALS results?
- How a variation in the beam energy affects the time resolution and shape of the resolution curve, and finally affect the precision of extraction of positron lifetime values?

- How important is the level of background and the uncertainties in its shape used for the fitting procedure;
- Can one improve the accuracy by simulating depth-profiling distributions of positrons stopped in the sample?

Efforts to develop more precise Monte Carlo simulations are in progress, in order to solve these and other questions.

In general, the first preliminary results on this PALS detector are positive and promising. We intend to develop this project further with the final goal to use it for PALS measurements of thin films in the near future.

Acknowledgments

The authors wish to express their gratitude to Region Rhône-Alpe and CEA-LETI for supporting this research.

References

[1] Y.C. Jean, Material Sci. Forum **175-178** (1995) 59;
Positron Spectroscopy of Solids, edited by A. Dupasquier and A. P. Mills, Jr (IOS, Amsterdam, 1995) p.503.

[2] A.J. Hill, in: M.R. Tant et all (eds.), High temperature properties and applications of polymer materials, ACS Symposium Series, **Vol 603** (1996).

[3] H.J. Ache, in D.M. Schrader, Y.C. Jean (eds.), Positron and Positronium Chemistry, Elsevier, Holland, 1988, p. 318.

[4] O.E. Mogensen, Positron Annihilation in Chemistry, Springer Series in Chem. Phys.$V58$, Springer, Berlin, (1995).

[5] D. W. Gidley et al., Phys. Rev. **B 60**, R5157 (1999).

[6] P. Schultz and K. G. Lynn, Rev. Mod. Phys. **60**, 701 (1988).

[7] A. Rich, Rev. Mod. Phys. **53**, 127 (1981).

[8] L. Xie at el., Phys. Rev. Lett. **74**, 4947 (1995).

[9] G. B. DeMaggio et al., Phys. Rev. Lett. **78**, 1524 (1997).

[10] D. Schodlbauer et al., Positron Annihilation edited by P.C. Jain et al., World Scientific, Singapore, 1985, p. 957.

[11] R. Suzuki et al., Material Sci. Forum **105-110** 1992 (1992).

[12] See, for example, J. N. Sun, Y. F. Hu, W. E. Frieze, D. W. Gidley, Rad. Phys and Chem., **68**, 351 (2003), and references therein.

[13] B. Jaskel, W. Westmeier and P. Patzelt, Nucl. Instr. Meth. **A 261**, 543 (1987).

[14] *Positron Spectroscopy of Solids*, edited by A. Dupasquier and A. P. Mills, Jr (IOS, Amsterdam, 1995).

[15] The program has been used to calculate magnetic fields in Tritsk Electron Neutrino Mass experiment.

[16] Rulon Mayer and Alex Weiss, Phys. Rev **B 38**, 11 927, (1988);
K. Nashimura, J. Kavata, and K. Ohya, Nucl. Instr. Meth. **B 164**, 903 (2000)
K. Ohya et al., Japan J. Appl. Phys. **35** 6226 (1996).

[17] N. Overton and P.G. Coleman, Phys. Rev. Lett. **79** 305, (1997).

[18] K. F. Canter, A. P. Mills, Jr., and S. Berko, Phys. Rev. Lett. **33**, 7 (1974).

[19] W. E. Frieze, D. W. Gidley, and K. G. Lynn, Phys. Rev. **B31**, 5628 (1985).

[20] The simulation programm is based on GEANT 3.21, CERN Program Library Long Writeup W5013.

[21] R. Paulin and G. Ambrosino, J. Phys. (Paris) **29** 263 (1968).

[22] W. Brandt and R. Paulin, Phys. Rev. Lett. 21 (1968) 193; Phys. Rev. **B5**, 2430 (1972).

[23] R. A. Lindy, Phys. Rev. **125**, 1686 (1962).

[24] K. F. Canter, A. P. Mills, Jr., and S. Berko, Phys. Rev. Lett. **33**, 7 (1974).

[25] H. von Busch et al., Phys. Lett. **B325**, 300 (1994).

[26] EG&G ORTEC "Model 462 Time Calibrattor Operating and Service Manual", 1996.

[27] Application Software Group, MINUIT Reference Manual, CERN Library **D506** (1992).

[28] PATFIT-88, Riso National Lab., Denmark.

[29] R.B. Gregory, J. Appl. Phys. **70** (1991) 4665.

[30] A. Shulka, M. Peter, L. Hoffmann, Nucl. Instr. and Meth. **A 335** (1993) 310.

[31] J. Kansy, Nucl. Instr. and Meth. **A 374** (1996) 235.